Design and parametric analysis of a wide-angle polarization-insensitive metamaterial absorber with a star shape resonator for optical wavelength applications

Sultan Mahmud[a,b,*], Sikder Sunbeam Islam[a], Kamarulzaman Mat[b], Muhammad E.H. Chowdhury[c], Hatem Rmili[d], Mohammad Tariqul Islam[b,*]

[a] Department of Electrical and Electronic Engineering, International Islamic University Chittagong, Bangladesh
[b] Department of Electrical, Electronic & Systems Engineering, Faculty of Engineering and Built Environment, Universiti Kebangsaan Malaysia, 43600 Bangi, Selangor, Malaysia
[c] Department of Electrical Engineering, Qatar University, Doha 2713, Qatar
[d] King Abdulaziz University, Faculty of Engineering, Electrical and Computer Engineering Department, P.O. Box 80204, Jeddah 21589, Saudi Arabia

ARTICLE INFO

ABSTRACT

Optical wavelengths considered as the key source of electromagnetic waves from the sun, and metamaterial absorber (MMA) enables various applications for this region like real invisible cloaks, color imaging, magnetic resonance imaging, light trapping, plasmonic sensor, light detector, and thermal imaging applications. Contemplated those applications, a new wide-angle, polarization-insensitive MMA is presented in this study. The absorber was formatted with three layers that consisted of a sandwiched metal-dielectric-metal structure. This formation of metamaterial absorber showed a good impedance match with plasmonic resonance characteristics. The structure was simulated using the FIT and validated with the FEM. A variety of parametric studies were performed with the design to gain best physical dimension. The mechanism of absorption also explained immensely by various significant analysis. The design had average 96.77% absorption from wavelengths of 389.34 nm to 697.19 nm and a near-perfect absorption of 99.99% at a wavelength of 545.73 nm for TEM mode. For an ultra-wide bandwidth of 102 nm, the design exhibited above 99% absorbance. The proposed is wide-angle independent up to 60° for both TE and TM mode, which is useful for solar energy harvesting, solar cell, and solar thermophotovoltaics (STPV). This MMA can be used for an optical sensor or as a light detector. Moreover, this proposed design can be employed in some applications mentioned above.

Introduction

After V. Veselago's theoretical explanation in 1967, Smith et al. illustrated a double negative (DNG) metamaterial with negative permeability and permittivity [1,2]. For significant variations at the operational frequencies of the metamaterials, the free space wavelength should be kept high in the design of a unit cell [3]. These kinds of metamaterials properties depend on their physical structure rather than their chemical characteristics with uses like invisible cloak [4], antenna [5], absorber [6], specific absorption rate (SAR) reduction [7], superlenses [8], filter [9,10], waveguides [11], imaging [12,13], determine physical properties [14], sensors [15–22]. Metamaterials give the benefit of interacting with the EM waves with a substance by artificially designing or review a unit cell, enabling a wide variety of absorbing applications [23–25]. Due to the periodic structure of a metamaterial absorber (MMA), its absorbance is high, and is it will absorb high frequency instead of the small thickness of the unit cell [26,27]. An absorber can be described as a perfect or near unity absorber if it can absorb all the incident radiation that falls into it. In the phenomenon of transmissivity, scattering, reflectivity, and further light propagation channels are ineligible. At specific wavelengths, resonant absorbers rely on materials and incident radiation [28]. Perfect absorbers indicate that the real part of the magnetic permeability must be equal to the real part of the electrical permittivity, and the imaginary part should be much more significant to dissipate the maximum energy of the EM wave of the PA medium [29]. The

* Corresponding authors at: Department of Electrical and Electronic Engineering, International Islamic University Chittagong, Bangladesh (S. Mahmud); Department of Electrical, Electronic & Systems Engineering, Faculty of Engineering and Built Environment, Universiti Kebangsaan Malaysia, 43600 Bangi, Selangor, Malaysia (M.T. Islam).

E-mail addresses: sultaniiuc3ni@gmail.com (S. Mahmud), tariqul@ukm.edu.my (M.T. Islam).

absorbance of the material-based absorber [30,31] was high because of its periodic structure. For this reason, unlike low thickness materials, this material could absorb high-frequency from terahertz to infrared with a more comfortable and less costly fabrication process [32–35]. The main reason for a broadband near-perfect absorber is the impedance match of plasmonic metamaterials with the confinement of waves by dielectric and resonator layer. Perfect resonance characteristics of the dielectric layer also a very good reason for high absorption [36,37]. A high thickness metal layer also helps any MMA to eradicate the transmission and to obstruct the light completely [38]. A stable dielectric constant substance will help a unit cell design to achieve a high resonance wavelength said by Landy et al. when they first exhibit an MMA. They found almost 88% absorbance at 11.5 GHz by using FR-4 and copper [39]. In the same year, Tao et al. introduced the first Terahertz MMA, which has 70% absorption at 1.3 THz [37].

The first broadband perfect absorber (MMA) was introduced by Lee et al. in 2012. Using FR4 as the dielectric layer along with copper as the metal layer, these researchers measured a 99.5% absorbance at 13.5 GHz [29]. A new type of MMA designed with a periodic array of the sandwiched dielectric cylinder of Si with Metal Ni, which found above 90% absorption for the full optical region and above 99% from 500 nm to 560 nm for transverse electric (TE) and transverse magnetic (TM) mode [40]. A three-layer metamaterial absorber with a fish-scale structure having above 70% average absorption for the whole visible spectrum consisted of silver and fused quartz for TE and TM mode [41]. Metasurface based three-layer MMA consisted of metal-dielectric-metal found average 83% absorption in full visible wavelength with a peak of 92% absorption [42]. Nearly perfect absorption of an average of 80% in the visible wavelength of 400 nm to 700 nm was found with the Cu/Si3N4/Cu stack layer on a silicon substrate [43]. A four-layer dual-band absorber with gold, gallium arsenide (GaAs), and pyrex (glass)evidenced 99.99% and 99.90% absorbance [44]. A three-layer absorber using a slender silicon dioxide (SiO$_2$) plane separating two gold metal planes executed a higher than 90% absorbance in visible and IR regimes [45]. Al-SiO$_2$-Al based three-layer MMA exhibited an average 95% absorption from 450 nm to 600 nm in visible wavelength [46]. A three-layer absorber using gold–silicon dioxide-gold had broadband over 90% absorption in the visible wavelength range and IR regimes at both polarization using a genetic algorithm (GA) for TE and TM mode [47]. A two-layer MMA structure consists of metal gold (Au) and diamond shape dielectric silicon (Si), which have above 93.3% absorptivity in full visible ranges with peak 99.1% at the 453 nm wavelength [48]. An ultra-broadband MMA formed of a repetitive array of metallic–dielectric multi-layer edconical frustums that consisted of seven homogeneous metallic or dielectric pairs had an absorption efficiency of 80% from 474.4 nm to 784.4 nm for TE and TM mode up to 55° incident angle [49]. An ultrathin three-layer absorber with a 300 nm bandwidth consisting of Silver-SiO$_2$-Silver had an absorption above 80% with a peak value of around 98% [50]. An organic thin-film with aluminum (Al) resonator and indium tin oxide (ITO) gave an absorption of over 90% for a wide bandwidth of 100 nm using P3HT, PCBM, and P3HT:PCBM hetero-structures [51]. A tungsten-based MMA with SiO$_2$ as dielectric layer demonstrated an average 96.7% absorption for the whole visible spectrum has been proposed by Mahmud et al [52].

Metamaterial absorber also can be found in other frequency ranges like Hz [53], KHz [54], MHz [55], GHz [56], THz [57,58], UV [59], IR [60,61] along with visible ranges vastly discussed above, with various uses like light trapping [62], light absorption switch [63], sound absorption [54], underwater sound absorption [64], photodetector [65], state of art [66], magnetic resonance imaging [67], solar cell [68], communication system [69], sensors [70–74], energy harvesting [75,76]. detector [77], waveguide [78], metal grids [79], filter [80], cryptography [81], antenna [82], THz light detection [83], integrated photonic circuits [84], solar thermophotovoltaics [85], stealth technology [86]. As the above discussion shows, Broadband near-perfect absorbers that cover the entire optical wavelength with more than 90%

absorption at all points are rare. However, using MMAs in the optical wavelength is desirable with various applications.

A new MMA has been designed is this work, which is composed of metal-dielectric-metal ultrathin nanostructure called metasurface form 389.34 nm to 697.19 nm wavelengths (430THz to 770THz) and analyzed it in TEM, TE, and TM mode. Previous literature reviews indicate that broadband MMAs with wide-angle and above 95% average absorption in the optical region is not readily procurable. Adopting tungsten helps the proposed design to withstand high temperatures, and its impedance is matched with the free space for the optical spectrum. Silicon-dioxide is also used to benefit the design because it has low relative permittivity with lossless characteristics in the optical region and a high melting point. Plasmonic resonance characteristics are also generated by this proposed geometrical structure for the whole spectrum. Optical wavelengths considered as the primary source of the sun's electromagnetic emission. The unit cell design is simulated in FIT and verified it with FEM. Here, the MMA has the highest absorption, which is 99.99% at 545.73 nm and an average 96.77% absorption for the full optical spectrum. It had up to 99% absorption in a wideband between 498 nm and 600 nm. To determine the best absorbance and mechanisms of the MMA, we changed the shape by tuning the parameters of the unit cells. The real part of the normalized impedance of this design meets to unity, and the imaginary parts to zero are the main reason for the MMA to exhibit this kind of high absorption. There is some other important mechanism that works for the high absorbance, which has been discussed later.

Design and simulation setup

Materials choice and design procedure

Approaching an MMA with materials like excellent optical properties along with high-temperature resistance is the main discomfort nowadays. Although broadband near-perfect absorber with plasmonic materials is ongoing work. For eliminating these discomfort, a new MMA design has been proposed, which was composed of a resonator and a metallic plane made with tungsten (Wolfram [W]), and the dielectric layer was made with lossless silicon dioxide (SiO$_2$), respectively. In the simulation process W (optical, Palik) and SiO$_2$ (optical, Ghosh) dispersion equations, optical properties, and band structures were taken from reference [87] and [88,89], respectively. The main reasons for choosing tungsten as metal-layer and resonator because of its high impedance matched with the free space in the optical spectrum and high intrinsic losses, which decrease the reflection and transmission near to zero. Also, tungsten itself shows high absorptivity in the optical region. Lossless characteristics of SiO$_2$ give us the intention to choose it as the dielectric spacer. MMA shows very high absorption if the dielectric constant of the dielectric layer has a large imaginary part for the whole broadband. Its resonance characteristics also help the design to impedance match. However, as it is nearly lossless in the optical wavelength region, any absorption with itself was ignored. For capturing the resonance wavelength, the geometrical structure also plays a vital role. So, the designed resonator varied by utilizing various metamaterial shapes, such as a cross, sawtooth, and star shape, hour-glass shape, nanorod, meander-ring, stacked, split-ring, double asterisk shape with utilizing organic and inorganic film [90–102] for tuning the absorption. The resonator resembled a cross shape with three cylindrical in it, which produced a star shape resonator (SSR) was used in our proposed design.

Fig. 1, (a) - (d) showing the steps of the design procedure for the proposed structure and (e) showing the three-dimensional view of the final design where (f) and (g) showing the physical dimension of the proposed structure with the front and the side views. The design used an SSR, which is a very good symmetrical structure, proved later. The width and length of the structure were 1000 nm, and the thickness of the SSR, dielectric layer, and a metal plane was 15, 60, 150 nm,
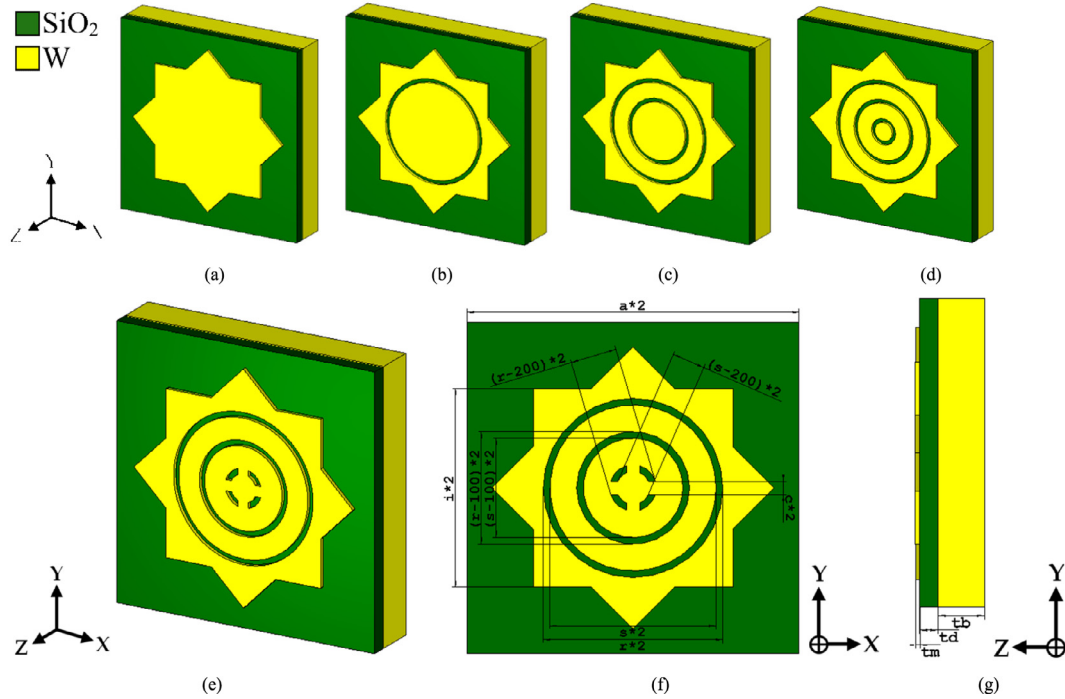
Fig. 1. The design procedure of the unit cell with three-dimensional view of (a) step-1, (b) step-2, (c) step-3, (d) step-4, and (e) final proposed design and physical dimension of the structure from (f) front view from z-axis and (g) side view from x-axis.

Table 1
Parameters list of the unit cell.

Parameter	r	s	c	a	l	i	tb	td	tm
Value (nm)	270	250	20	500	70	300	150	160	15

respectively. In step 1 two square boxes of width and length of 600 nm inserted in the top of the dielectric layer with a 45-degree angle between them. Then in step 2, cylindrical circular cuts of outer radius 270 nm and inner radius 250 nm implemented in the resonator. In step 3 and 4 cylindrical cuts of outer radius 170 nm and 70 nm with inner radius, 150 nm and 50 nm applied in the resonator, respectively. Then in the final step, a cross shape of with 40 nm and length 140 nm enact in the design which completed the design procedure for the resonator. The dimensions with the best parameter values were achieved using parameter sweep. As the total thickness is bound to 225 nm of the structure, which is ultrathin, it can be easily used as a sheet to roll over any photovoltaic (PV) cell-like solar thermos-photovoltaics (STPV) for solar energy harvesting. Due to the theoretical studies estimating efficiencies up to 85%, STPV will be highly useful for future applications. Also, the high-temperature stability of the materials will make the design efficient and effective for practical STPV applications though the thicknesses are very low, and the structure is in the nanometer scale [103]. Note that, in Fig. 1, W represents as yellow color and SiO_2 as olive color. The design parameters are listed in Table 1 below.

Simulation setup

Here a unit cell of the proposed design has been simulated with periodic boundary conditions to evaluate the results and for further discussion. Perfect electric conductor (PEC) and perfect magnetic conductor (PMC) were taken for y-z and x-z planes, respectively, in the simulation process for TEM. The z-axis was considered an open space where the linearly polarized planar wave would pass through the structure from the front side. The x-axis and y-axis were taken as an electric boundary and magnetic boundary, respectively. The boundary

condition was sufficient to obstruct the near field difficulty. The electric and magnetic fields and direction of propagation followed the $\times$, y, and z directions, respectively. Here, the electric field, the magnetic field, and the open space were perpendicular to each other. For TE and TM mode, the floquet port with master and slave has been used. For the simulation and the results of the absorber and parameter sweep, CST microwave studio has been used, which is based on the FIT. Further data analysis was conducted, and a graph was produced with CST-MATLAB interference demonstrated in the results and discussion section.

Results and discussion

Methodology and absorbance of the proposed unit cell

From the S parameters, effective permittivity and permeability have been extracted by using the Nicolson-Ross-Weir (NRW) equation [104]. Wave phases, reflection, and transmission magnitudes were used to obtain the S parameters. The absorption response of the proposed structure $A(\omega)$ could be calculated using the absorption equation. The Absorption $A(\omega)$ formula was:

$$A(\omega) = 1 - R(\omega) - T(\omega) = 1 - |S_{11}(\omega)|^2 - |S_{21}(\omega)|^2 \qquad (1)$$

here, the Reflection, $R(\omega) = |S_{11}(\omega)|^2$ and Transmission, $T(\omega) = |S_{21}(\omega)|^2$.

Here, the impedance of the proposed unit cell is $Z(\omega)$, which can be measured from eq. (2), and characteristics impedance from eq. (3).

$$Z(\omega) = \{\mu_r(\omega).\mu_0/[\varepsilon_r(\omega).\varepsilon_0]\}^{1/2} \qquad (2)$$

$$Z_0 = (\mu_0/\varepsilon_r)^{1/2} = 376.73 \approx 377\ \Omega \qquad (3)$$

here, μ_0 = vacuum permeability, ε_0 = vacuum permittivity, μ_r = relative permeability, and ε_r = relative permittivity.

If the intrinsic impedance is equal to free space impedance ($Z(\omega) = Z_o$) by adjusting the geometric shape of the resonator and size of the structure, the absorption will be near unity or unity. Also, absorption is inversely proportional to reflectance and transmittance. These
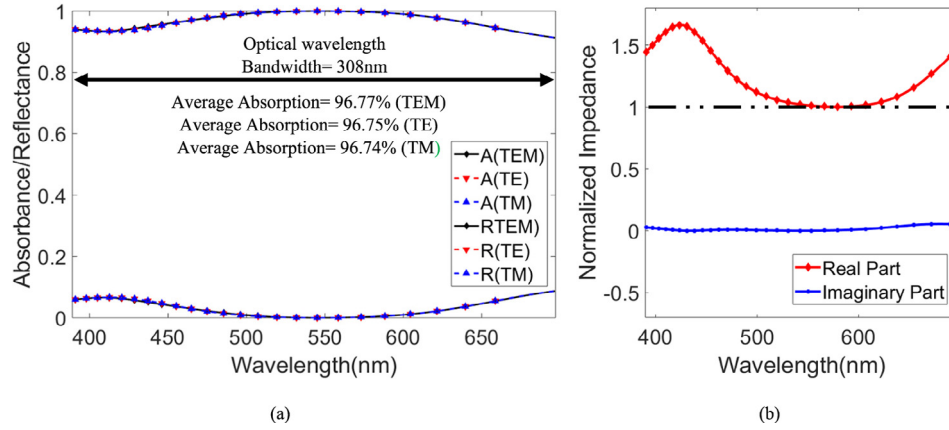
Fig. 2. Graphical representation of (a) absorbance, and reflectance for TEM, TE, and TM mode (b) real and imaginary parts of normalized impedance for the proposed design in linear scale.

values are frequency-dependent because of their dispersive properties. However, as tungsten blocks the maximum transmittance (T(ω)), so the transmission T(ω) is too small, and the absorption is proportional to reflection R(ω). So absorption can be extracted by evaluating eq. (4).

$$A(\omega) = 1 - R(\omega) = 1 - |S_{11}(\omega)|^2 \qquad (4)$$

here, $|S_{21}|^2 = 0$, as T(ω) is very closed to zero.

Fig. 2(a), demonstrated the absorbance, reflectance, and transmittance for the given dimensions with tungsten and silicon dioxide. As mentioned earlier, the impedance match is shown in Fig. 2(b). If the real part of the normalized impedance is near unity and the imaginary part is near zero, then it will make a metamaterial to a near-perfect absorber. Both phenomenon are illustrated in the proposed design, which can be seen from Fig. 2(b). The proposed structure had 99.99% absorption at 545.73 nm and above 99% absorption from 599.53 nm to 497.6533 nm with a wide bandwidth of 102 nm. It had absorption significantly higher than 91.24% in the all-optical region from 389.19 nm to 697.39 nm with an average 96.77% absorption. The design shows 32% better energy absorption than lossy semiconductor or metal absorbers.

In this proposed structure, tungsten is used as a metal plane and shows an excellent impedance match with free space. Also, Surface plasmons of tungsten do not exist in optical wavelengths. As can be seen, the value of Z_0 was slightly lower than the value of Z(ω) and showed near-perfect absorption. An absorber of this kind has the potential to act as a super absorber. The incident wave was confined by the structure and shows a good absorbance for high bandwidths. The back-layer metal plane prevents the incident waves caused low transmission, and the front-layer also absorbs the waves with the resonator and dielectric layer. Here, SiO_2 helps to minimize the distance of the wave because of its low thickness. Intrinsic losses in the front-layer and resonance characteristics in the dielectric layer also help in perceiving the impedance match with free space in the optical region. These phenomena are the reason for the proper infiltration of the wave and high-performance absorber. However, these all phenomena may not be able to exhibit this kind of higher absorption if the SSR with three circular cuts had not been used. For high absorption, the incident wave must be confined by the MMA structure. The SSR helps the structure to confine the wave with complex dispersion. The resonator reflects the wave from the front end as back-layer metal reflects the wave from the back end.

However, one question always arises when designing an MMA that is the MMA converting the polarized wave instead of good absorptivity. For diminishing the question, co-polarization and cross-polarization phenomenon demonstrated here with the polarization conversion ratio (PCR). Co-polarization and cross-polarization components can be measured form eq. (5) and (6) demonstrated in Fig. 3(a).

$$|S_{11}(\omega)|^2 = |R_{yy}|^2 + |R_{yx}|^2 \qquad (5)$$

$$|S_{11}(\omega)|^2 = |R_{xx}|^2 + |R_{xy}|^2 \qquad (6)$$

Here, R_{yx} and R_{xy} is the cross-polarization component, R_{xx} and R_{yy} is the co-polarization component. Using the linear value of R_{yy}, R_{yx}, R_{xy}, and R_{xx} PCR can be calculated by using eq. (7) and (8) exhibited in Fig. 3(b).

$$PCR_{TE} = R_{yx}^2/(R_{yy}^2 + R_{yx}^2) \qquad (7)$$

$$PCR_{TM} = R_{xy}^2/(R_{xx}^2 + R_{xy}^2) \qquad (8)$$

From Fig. 3, it can be readily comprehensible that, the design it not converting the polarization wave, and the PCR value is near zero for both modes. Excellent symmetrical SSR is the main reason for this kind of result.

To grasp the absorption characteristics with the structure, it was separated into two layers. The front-layer was comprised of a metal resonator along with a dielectric substrate (SiO_2), and the back-layer consisted of only a metal plane (tungsten). As shown in Fig. 4, the front-layer contributed more to the complete absorption, while the back-layer also contributed a subsidiary. At 584 nm wavelength, the absorption level rhymed with each other but then detached. The front-layer absorption was consistent then back layer absorption in the proposed structure. The back-layer was made with tungsten, and the impedance match with the free space in the optical wavelength was the main reason for this. In the front-layer, the capacitive and inductive properties of the resonator and the lossless characteristics of silicon dioxide were the reason for the absorption. Though SiO_2 absorption ignored, it shows excellent absorption composed of a metal resonator.

To validate the simulated data (FIT) with tungsten and SiO_2, the simulation of the proposed design with the finite element method (FEM) in ANSYS high-frequency simulation software (HFSS) has been done here. In Fig. 5, the comparison of the acquired data from CST and HFSS is shown. Peak absorption remains almost the same at 99.99%, and the average absorption is above 89.14% in the full visible wavelength. There was a small inconsistency in both simulated results, mainly because of the two different simulation environment setup. The optical properties of W and SiO2 also differ a little in both environments. Also, the refractive index of SiO2, which consider a very important parameter, was little different in both simulation setup for CST and HFSS in the full visible region. Moreover, the method of extracting s-parameters is also very different from each other, even a good reason for this kind of small inconsistency. However, the magnitude of the S_{11} parameter matched very well, which is a reason for the good match in the absorption level in both simulation setup.
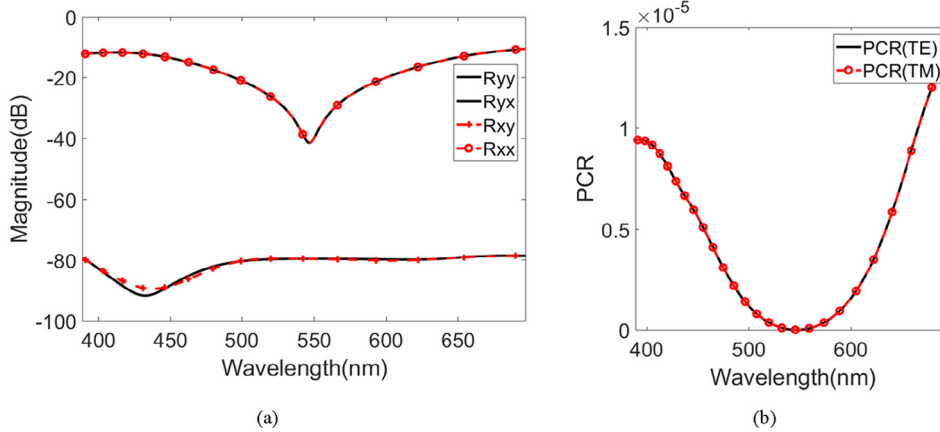
Fig. 3. Graphical representation of (a) co-polarization and cross-polarization component in magnitude (dB), and (b) polarization conversion ratio (PCR) for both TE and TM mode.
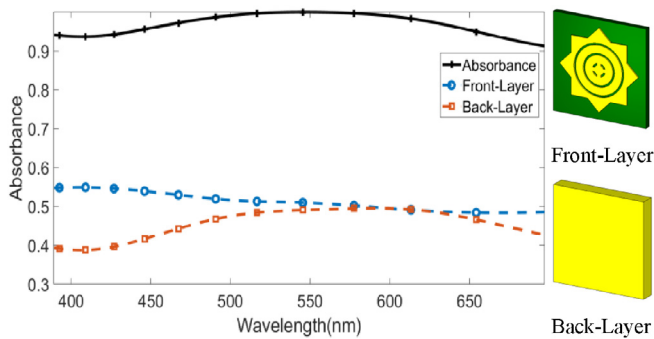

Fig. 4. Absorbance evaluation with front (resonator and dielectric) and back (metal) layers.
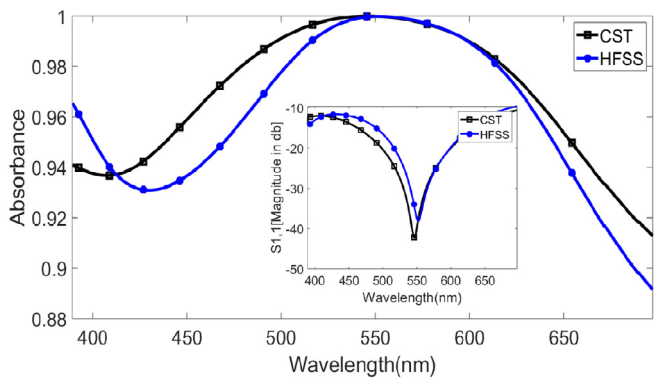

Fig. 5. Comparison of absorption with different simulation methods FIT and FEM, by CST and HFSS simulation software respectively. Insets: S_{11} parameter (magnitude (dB)) with both CST and HFSS simulation software.

Polarization and incident angle independency

As mentioned earlier that the design is wide-angle sensible; here in this section, the consequence will be proved. The design was under consideration for a different oblique angle for both TE and TM mode which has been demonstrated in Fig. 6, with the visual representation of the normal and oblique incident angle in Fig. 6(a) and (b). As the design is symmetrical (proved previously), different polarization angle hasn't affected the design, and the absorption remain same for angle 0-45° shoed in Fig. 6(c) and (e). However, different incident angles produced a different level of absorption for both TE and TM mode exhibited in Fig. 6(d) and (f). For TE mode, the incident angle increases stepwise from 0° to 60°. For 0° to 50°, the design showed almost average

absorption of around 95%, and for 60° it is decreased by 85.28%, but the absorptivity is remained up to 70%. And in TM mode, average absorption up to 96% for all incident angle from 0° to 60°. These two particular characteristics are very useful for uses in solar cells and solar energy harvesting and STPV, as it has known that the higher the incident angle, the higher the path length, the lower the coupling effect. This decreased coupling effect weakens the electromagnetic dipolar resonance for the structure, which caused the less confinement of the wave in the dielectric layer. But, in TM mode, the confinement hasn't affected as the wave component is parallel with the mode.

Parametric analysis of the unit cell

Here important parameter sweeps from Table 1, has been shown with their shape chance along with the graph. Parameter sweeps help determine the best absorbance and use of the design. The parameter sweep "c", "l", "tb", "a" were not expressed here as they did not demonstrate any meaningful consequences. The first parameter sweep was the parameter "r". By changing this parameter, the gap between the circular gaps increased and decreased. The effect of the circular gap "r" changed from 260 nm to 300 nm at an interval of 10 nm, and the results are shown in Fig. 7. This change involved five steps and changed the gap between the circular cylinders from 10 nm to 50 nm. There were three circular gaps in the design. The absorption magnitude for all values of the gap to the circular gap was above 99% at the resonance frequency. The best value we found was at a gap of 20 nm, which was at r = 270 nm. Here, the resonance wavelength shifted with the change in the gap between the shapes.

At the starting and end value, there was a slight up-down when parameter "i" changed, exhibited in Fig. 8. The resonance frequency differs skimpy but always dwell up to 99%. Successive increments of "i" decreased the self-inductance but increased the mutual inductance with the metal layer as the resonator shape increased. This mutual inductance increased the resonance wavelength linearly. This kind of parametric study helps us to determine the optimum size of the resonator.

A major variation was evident at the change of the parameter "td," which refers to the thickness of the dielectric material exhibited in Fig. 9. After altering the thicknesses from 40 to 80 nm, a major change in the absorbance has been observed, and the resonance wavelength also sweeps a lot. Dielectric layer thicknesses of 40, 50, 60, 70, and 80 nm showed resonance values of 97.15%, 99.47%, 99.99%, 99.78%, and 99.18%, respectively. A dielectric layer thickness varied the resonance wavelengths linearly at 452.24, 488.58, 545.73, 604.88, and 663.61 nm, respectively. The resonator capacitance change could explain this dielectric layer thickness variance with the parameter change.
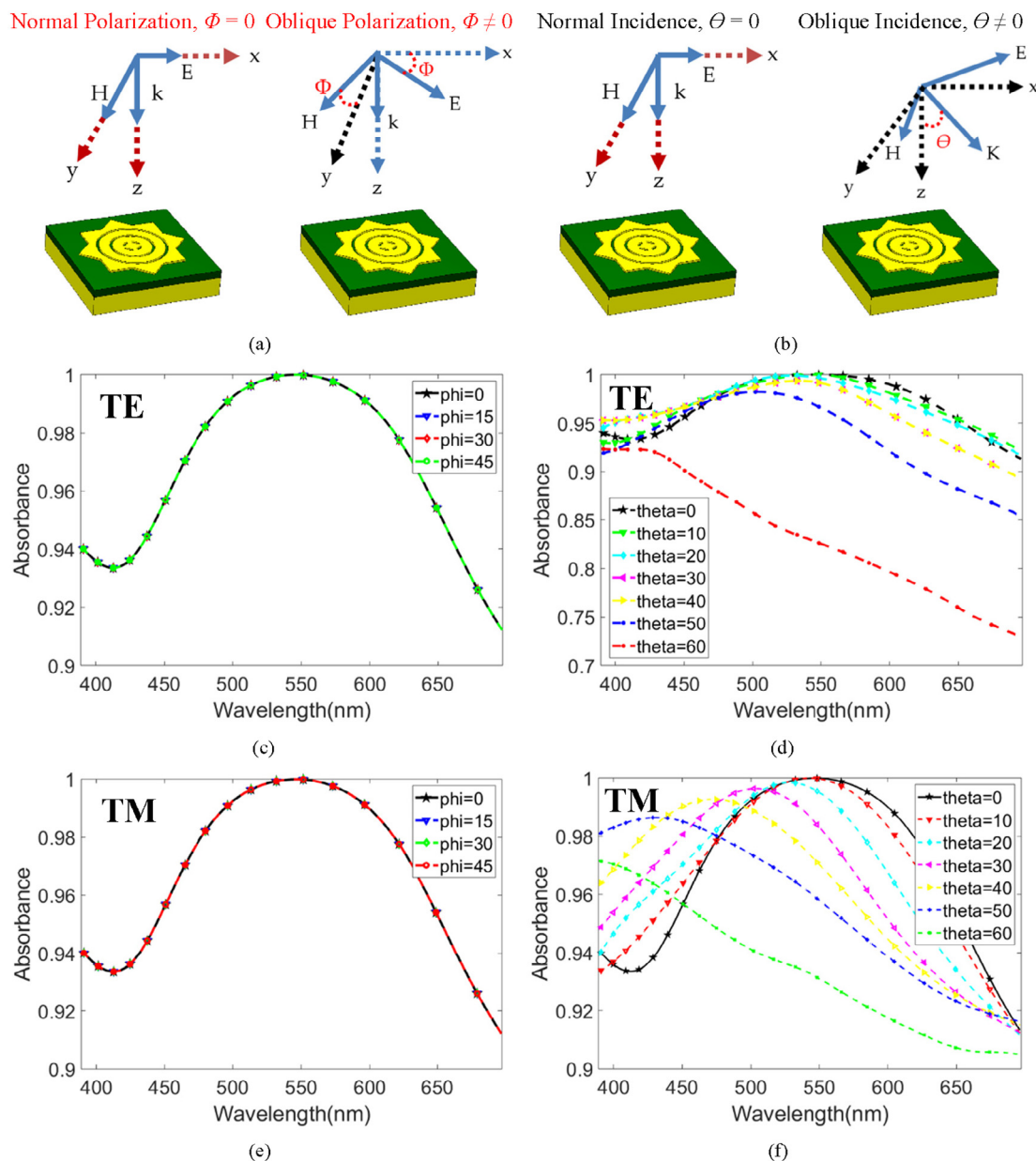
Fig. 6. (a) Visual representation of normal and oblique polarization angle, (d) normal and oblique incident angle, (c) absorbance for different polarization angle in the TE mode from 0 to 45°, (d) absorbance for different incident angle in the TE mode from 0 to 60°, (e) absorbance for different polarization angle in the TM mode from 0 to 45°, and (f) absorbance for different incident angle in the TM mode from 0 to 60°.
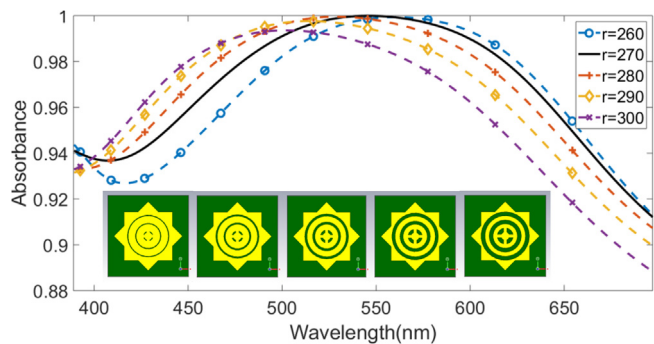

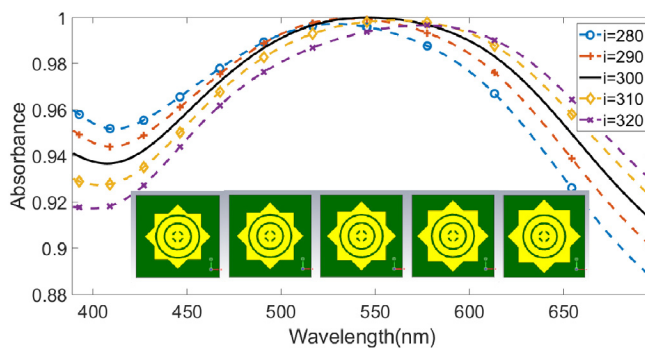**Fig. 7.** Absorption response for parameter sweep "r".

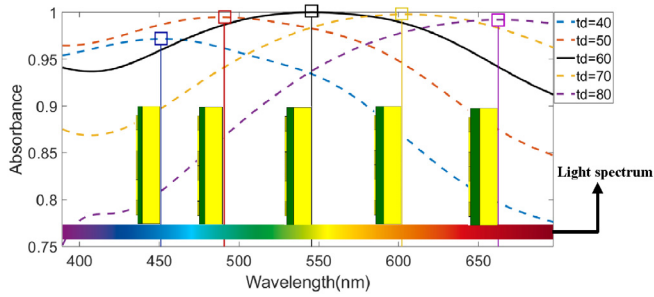**Fig. 8.** Absorption response for parameter sweep "i".

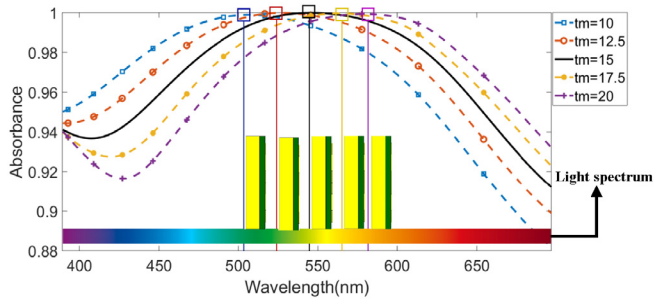**Fig. 9.** Absorption response for parameter "td".

Fig. 10. Absorption response for parameter "tm".

The capacitance value between the metal and resonator was inversely proportional to the dielectric layer thickness. The equivalent capacitance of the system was reduced as the upper metal structure capacitance was in series with others. The decrease in the capacitance increased the resonance frequency. The inductance and capacitance of the structure are thought to be responsible for this observation, as the resonance wavelength was seen to shift to the right as the dielectric material thickness increased. This phenomenon could be utilized in optical sensors or detect the thickness of any dielectric layer.

The last and vital parameter sweep involved sweeping the thickness of the resonator with "tm" which was altered from 10 nm to 20 nm with an interval of 2.5 nm, as shown in Fig. 10. As the resonator thickness increased, the resonance wavelength also shifts its position linearly. Here, the resonator illuminated to an electric field component of the electromagnetic field had an inductance. The resonator and metal created a capacitance and inductance that was proportional to increments in the thickness, and all resonance frequencies were greater than 99% at all thicknesses. The right shifts of resonance wavelengths with the change in the metal resonator thickness could also be observed.

Absorption with different dielectric materials

The material of the dielectric has been changed here, which shown in Fig. 11(a) with a different refractive index. Here, silicon dioxide, silicon nitride, silicon amorphous, gallium arsenide, and graphene has refractive index 1.5, 2.0, 4.4, 3.9, and 2.6, respectively. As it is known that lower the refractive index, the higher the absorbance and the larger the bandwidth [105]. As can be seen, a perfect result was found with SiO_2 as it has the lowest refractive index than others. Silicon nitride (Si_3N_4) showed unique results with a linear absorbance. This property enables this kind of structure to be improvised as a visible light detector because it shows different absorbances for individual colors of light. It may be used as an invisible cloak, as it absorbs the light spectrum efficiently. The other two results with silicon amorphous and gallium arsenide showed half-power absorbance in a wide range of wavelengths, which could be utilized in half power solar cell applications. With graphene, the absorbance exhibit over 74% in all-region. Varying the materials could also vary the application of the design of the same metamaterial.

The absorbance of glass (Pyrex) is shown in Fig. 11(b) which showed similarities to silicon nitride in Fig. 11(a). It could be used as a light detection sensor as its absorption level changed linearly with the change in wavelength. Assuming that there was a fall in blue light in the design with 470 nm, this would produce absorbance of around 70%. The absorption level would determine the color of the light, and the wavelength level and could be used to help devices or artificial intelligence robots detect color or wavelengths.

E-Field, H-field and surface current analysis

It is known that absorption characteristics and energy dissipation highly depend on the electromagnetic field and surface charge distribution. In this section mechanism of absorption based one-field, h-field and surface charge distribution will be discussed for three corresponding wavelength λ = 400 nm, λ = 545.73 nm, and λ = 690 nm. Here three-wavelength chosen as three different absorption level, λ = 400 nm (93.5% - mid-level), λ = 545.73 nm (99.99% - resonance), and λ = 690 nm (91.74% - low level). The high electromagnetic field has been created by the absorber, which was shown in Fig. 12, (a)–(f) for both TE and TM mode in wavelength λ = 400 nm, λ = 545.73 nm, and λ = 690 nm. From Fig. 12, (a), (c), (e) it can be seen the confinement of electric wave is done by dielectric layer very well. And, Fig. 12, (b), (d), (f), exhibited the good confinement of magnetic wave. They both created a very good dipolar moment for both TE and TM mode [106,107]. So, surface plasmons increased and created a very good polarization-insensitive absorber for both modes along with a good impedance match of tungsten. Also, the high dipolar moment is situated in the interference of the metal/dielectric caused a very good absorption level [108]. Here, the direction of propagation only changed
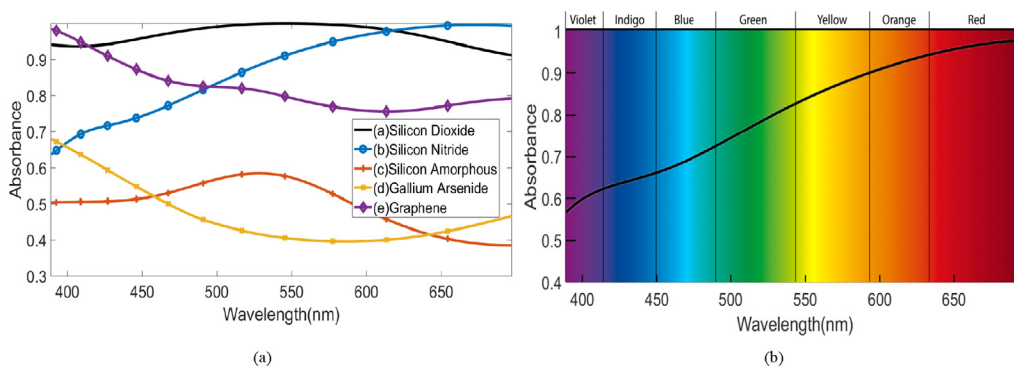

(a)

(b)

Fig. 11. (a) Absorption phenomenon with silicon dioxide, silicon nitride, silicon amorphous, gallium arsenide, and graphene as dielectric layer and (b) The illusion of increasing absorbance concerning wavelength in glass (Pyrex).
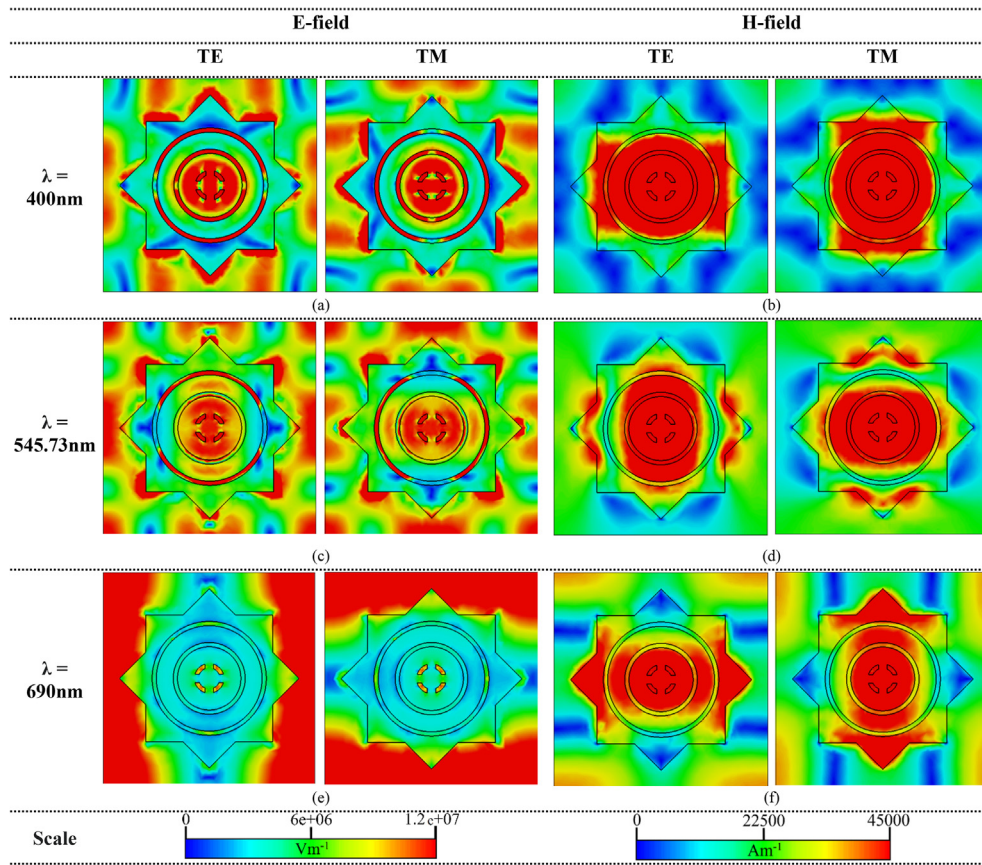
Fig. 12. Demonstration of E-field for TE and TM Mode in three wavelength (a) λ = 400 nm, (c) λ = 545.73 nm, and (e) λ = 690 nm in y-x axis and H-field for TE and TM Mode in three wavelength (b) λ = 400 nm, (d) λ = 545.73 nm, and (f) λ = 690 nm also in y-x axis with color bar scale.
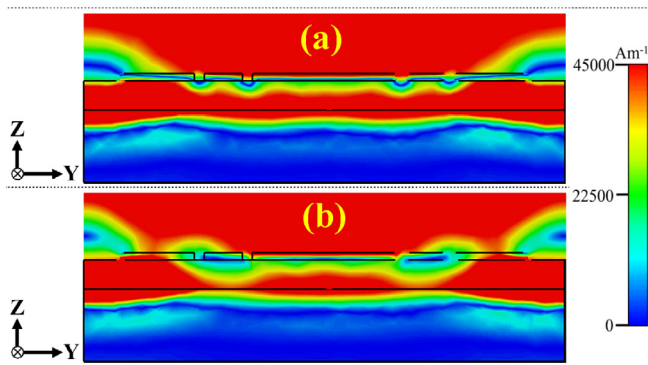

Fig. 13. The cross-sectional view of H-field in (a) TE mode and (b) TM for resonance wavelength 545.73 nm in z-y axis with the color bar scale.

concerning the change of EM mode. As discussed above, it was stated that the back-layer blocks the transmission as the metal is chosen in a particular thickness to do so. This phenomenon is seen from Fig. 13, (a), (b) for λ = 545.73 nm in TE and TM mode. It is also clearly to represent that the EM wave is mainly confined by the dielectric layer, not the metal layer. With good E-field and H-field, a good anti-parallel circulating current create in the structure showed in Fig. 14, (a)-(f). Surface charges are very highly distributed in the full structure, especially for the resonance wavelength, where they found the best results of peak 99.99% for TE and TM mode. The dipolar magnetic moment with the magnetic field, which causes a high electromagnetic field in the spacer layer, helps the design for fewer reflections [38,109]. From the above discussion, it can be clearly said that the design is a very good absorber for the whole optical region with high electromagnetic field and surface

current distribution, which will help it to use in related fields.

Comparative study

Table 2 discusses the comparison of previous designs (for optical wavelengths) with familiar features like bandwidth layer, dimensions. It can be easily procurable from the table that this work found an excellent absorption level compared with previous work with a wide-angle sensibility. Perfect optical wavelength absorbers that can operate in full regions are rarely found. Moreover, a rare nearly perfect absorbance with an average absorption of 96.77% with resonance absorbance of 99.99% in optical wavelengths was found in our design. A good impedance match of tungsten is one of the main reasons for high absorbance. In our proposed unit cell, we use a distinctive geometric shape with an SSR with three cylindrical cuts inside across, which also improves the absorption property from other designs we demonstrated below. Equivalent capacitance with the resonator and the back-layer metal is high too. High electromagnetic field and reasonable surface charge distribution differentiate our design from others. In terms of the extreme melting point of tungsten and SiO₂, low-materials cost, efficiency, and operational region compared with other materials used in the table below, makes this design a sole.

Conclusion

Broadband near-perfect polarization-insensitive, wide-angle MMA for optical wavelengths from 389.34 to 697.19 nm was designed in this study. The conventional methodology of three-layers with a metal-dielectric-metal structure was utilized. The structure showed a broad bandwidth and evidenced nearly perfect absorbance above 91.24% at all points with peak points of 99.99%. It also showed polarization and
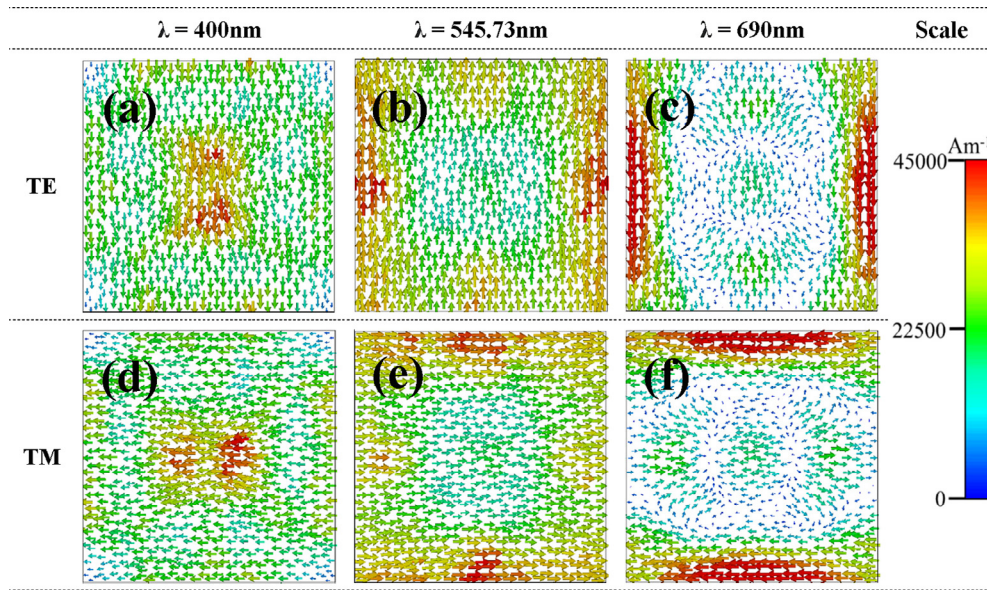
Fig. 14. Surface current distribution for wavelength (a) 400 nm, TE, (b) 545.73 nm, TE, (c) 690 nm, TE (d) 400 nm, TM, (e) 545.73 nm, TM, and (f) 690 nm, TM with the color bar scale.

Table 2
Comparative study on the previous and proposed design.

Ref. #	Bandwidth (nm)	Number of layers	Dimensions (l * w * h) in nm	Materials used	Polarization sensitivity & Angle (A ≥ 70%)	Absorption (%)	Peak value (%)
[40]	300	Three	250 * 250 * 350	Ni, Si	Yes, $\theta \le 60°$	Above 90	99
[41]	300	Three	380 * 380 * 235	Ag, SiO$_2$	Yes, $\theta \le 60°$	Above 90	98
[42]	380	Three	600 * 600 * 180	Au, SiO$_2$	No, N/A	Above 83	92
[43]	300	Four	Peridodic * 350	Cu, Si$_3$N$_4$, Si	No, N/A	Above 80	97
[48]	400	Two	240 * 240 * 170	Au, Si	Yes, $\theta \le 50°$	Above 90	99.1
[49]	310	Periodic array	500 * 500 * 600	Au, Si	Yes, $\theta \le 65°$	Above 80	98.5
[50]	300	Three	350 * 350 * 180	Ag, SiO$_2$	No, N/A	Above 80	98
[110]	350	Thee	Nanocomposite w = 182	Au, SiO$_2$, Al	Yes, $\theta \le 60°$	Above 80	99
This work	308	Three	1000 * 1000 * 225	W, SiO$_2$	Yes, $\theta \le 60°$	Above 91.24	99.99

incident angle independent behavior with an average 96.77% absorption. As a result of the good impedance match of tungsten and the lossless characteristics of silicon dioxide (SiO$_2$), better absorption was achieved with the structure. Investigations were performed with four other dielectric materials, and a variety of useful results were found. Using Si$_3$N$_4$ or glass (Pyrex) as dielectric substrates, the absorbance shifted linearly with the wavelength. Therefore, this structure may be applied as a light wavelength detection sensor. This metamaterial absorber could be utilized as an optical sensor, as it shifts its resonance along with the change in its dielectric layer and resonator thickness. Based on its angular independent characteristics, it may be utilized in solar energy harvesting applications or a solar sensor. The high melting point of the materials will be helpful to withstand the high temperature when the design absorbs photons from a higher energy source. However, the high melting points of the materials used in this study and the high absorbance of the broadband absorber could also be efficiently used in solar cells, optical sensors, real invisible cloaks, color imaging, and thermal imaging applications. The improved performance of these MMAs and their multiple potential applications open new doors in the optical wavelength paradigm.

CRediT authorship contribution statement

Sultan Mahmud: Conceptualization, Data curation, Formal analysis, Investigation, Methodology, Writing - original draft. **Sikder Sunbeam Islam:** Conceptualization, Data curation, Formal analysis, Investigation, Visualization, Writing - review & editing. **Kamarulzaman Mat:** Funding acquisition, Software, Writing - review & editing. **Muhammad E.H. Chowdhury:** Conceptualization, Software, Writing - review & editing. **Hatem Rmili:** Funding acquisition, Software, Writing - review & editing. **Mohammad Tariqul Islam:** Funding acquisition, Software, Supervision, Writing - review & editing.

Declaration of Competing Interest

The authors declare that they have no known competing financial interests or personal relationships that could have appeared to influence the work reported in this paper.

References

[1] V.G. Veselago The electrodynamics of substances with simultaneously negative values of ε and μ Sov Phys Uspekhi 1968 ,10(4)509 1968;509.

[2] Smith DR, Padilla WJ, Vier DC, Nemat-Nasser SC, Schultz S. Composite medium with simultaneously negative permeability and permittivity. Phys Rev Lett

2000;84:4184–7. https://doi.org/10.1103/PhysRevLett.84.4184.

[3] Smith DR, Vier DC, Koschny T, Soukoulis CM. Electromagnetic parameter retrieval from inhomogeneous metamaterials. Phys Rev E - Stat Nonlinear, Soft Matter Phys 2005;71:1–11. https://doi.org/10.1103/PhysRevE.71.036617.

[4] Islam SS, Faruque MRI, Islam MT. A near zero refractive index metamaterial for electromagnetic invisibility cloaking operation. Materials (Basel) 2015;8:4790–804. https://doi.org/10.3390/ma8084790.

[5] Hasan MM, Rahman M, Faruque MRI, Islam MT, Khandaker MU. Electrically compact srr-loaded metamaterial inspired quad band antenna for bluetooth/wifi/wlan/wimax system. Electron 2019;8.. https://doi.org/10.3390/electronics8070790.

[6] Rana AS, Mehmood MQ, Jeong H, Kim I, Rho J. Tungsten-based Ultrathin Absorber for Visible Regime. Sci Rep 2018;8:2–9. https://doi.org/10.1038/s41598-018-20748-9.

[7] Faruque MRI, Islam MT. Design of miniaturized double-negative material for specific absorption rate reduction in human head. PLoS ONE 2014;9.. https://doi.org/10.1371/journal.pone.0109947.

[8] Zhang X, Liu Z. Superlenses to overcome the diffraction limit. Nat Mater 2008;7:435–41. https://doi.org/10.1038/nmat2141.

[9] E. Ahamed Faruque mohammad rashed iqbal, Alam M jubaer, Mansor mohd fais bin, Islam mohammad tariqul. Digital metamaterial filter for encoding information Sci Rep 2020:1–09. 10.1038/s41598-020-60170-8.

[10] Alam J, Faruque MRI, Islam MT. Labyrinth double split open loop resonator based bandpass filter design for S, C and X-band application. J Phys D Appl Phys 2018;51.. https://doi.org/10.1088/1361-6463/aac569.

[11] Smolyaninov II, Smolyaninova VN, Kildishev AV, Shalaev VM. Anisotropic metamaterials emulated by tapered waveguides: Application to optical cloaking. Phys Rev Lett 2009;102:1–4. https://doi.org/10.1103/PhysRevLett.102.213901.

[12] Islam MT, Samsuzzaman M, Islam MT, Kibria S. Experimental breast phantom imaging with metamaterial-inspired nine-antenna sensor array. Sensors (Switzerland) 2018;18.. https://doi.org/10.3390/s18124427.

[13] Mahmud MZ, Islam MT, Misran N, Singh MJ, Mat K. A negative index metamaterial to enhance the performance of miniaturized UWB antenna for microwave imaging applications. Appl Sci 2017;7.. https://doi.org/10.3390/app7111149.

[14] Karaaslan, Muharrem & Unal, Emin & Akgol, Oguzhan & Sevim, Umur & Öztürk M. Determination of Physical Properties of Concrete by Using Microwave Nondestructive Techniques. Appl Comput Electromagn Soc 2018;33:2018.

[15] Islam MT, Bin Ashraf F, Alam T, Misran N, Bin Mat K. A compact ultrawideband antenna based on hexagonal split-ring resonator for pH sensor application. Sensors (Switzerland) 2018;18.. https://doi.org/10.3390/s18092959.

[16] Kim HK, Lee D, Lim S. A fluidically tunable metasurface absorber for flexible large-scale wireless ethanol sensor applications. Sensors (Switzerland) 2016;16.. https://doi.org/10.3390/s16081246.

[17] Islam MT, Hoque A, Almutairi AF, Amin N. Left-handed metamaterial-inspired unit cell for S-Band glucose sensing application. Sensors (Switzerland) 2019;19:1–12. https://doi.org/10.3390/s19010169.

[18] Lu F, Tan Q, Ji Y, Guo Q, Guo Y, Xiong J. A novel metamaterial inspired high-temperature microwave sensor in harsh environments. Sensors (Switzerland) 2018;18.. https://doi.org/10.3390/s18092879.

[19] Cheng Y, Zhang H, Mao XS, Gong R. Dual-band plasmonic perfect absorber based on all-metal nanostructure for refractive index sensing application. Mater Lett 2018. https://doi.org/10.1016/j.matlet.2018.02.078.

[20] Wang Ben-Xin, Zhai Xiang, Wang Gui-Zhen, Huang Wei-Qing, Wang Ling-Ling. A novel dual-band terahertz metamaterial absorber for a sensor application. J Appl Phys 2015;117(1):014504. https://doi.org/10.1063/1.4905261.

[21] Karatepe A, Akgöl O, Abdulkarim YI, Dalgac Ş, Muhammadsharif FF, Awl HN, et al. Multipurpose chemical liquid sensing applications by microwave approach. PLoS ONE 2020;15:1–14. https://doi.org/10.1371/journal.pone.0232460.

[22] Abdulkarim YI, Deng L, Karaaslan M, Dalgaç Ş, Mahmud RH, Alkurt FO, et al. The detection of chemical materials with a metamaterial-based sensor incorporating oval wing resonators. Electron 2020;9.. https://doi.org/10.3390/electronics9050825.

[23] Salim A, Lim S. Review of recent metamaterial microfluidic sensors. Sensors (Switzerland) 2018;18. https://doi.org/10.3390/s18010232.

[24] Lee Y, Kim SJ, Park H, Lee B. Metamaterials and metasurfaces for sensor applications. Sensors (Switzerland) 2017;17. https://doi.org/10.3390/s17081726.

[25] RoyChoudhury S, Rawat V, Jalal AH, Kale SN, Bhansali S. Recent advances in metamaterial split-ring-resonator circuits as biosensors and therapeutic agents. Biosens Bioelectron 2016;86:595–608. https://doi.org/10.1016/j.bios.2016.07.020.

[26] Wang Y, Sun T, Paudel T, Zhang Y, Ren Z, Kempa K. Metamaterial-plasmonic absorber structure for high efficiency amorphous silicon solar cells. Nano Lett 2012;12:440–5. https://doi.org/10.1021/nl203763k.

[27] Vora A, Gwamuri J, Pala N, Kulkarni A, Pearce JM, Güney DO. Exchanging ohmic losses in metamaterial absorbers with useful optical absorption for photovoltaics. Sci Rep 2014;4:1–13. https://doi.org/10.1038/srep04901.

[28] C.M. Watts X. Liu W.J. Padilla Metamaterial electromagnetic wave absorbers Adv Mater 2012;24. 10.1002/adma.201200674.

[29] Lee YP, Tuong PV, Zheng HY, Rhee JY, Jang WH. An application of metamaterials: Perfect absorbers. J Korean Phys Soc 2012;60:1203–6. https://doi.org/10.3938/jkps.60.1203.

[30] Nguyen TT, Lim S. Wide Incidence Angle-Insensitive Metamaterial Absorber for Both TE and TM Polarization using Eight-Circular-Sector. Sci Rep 2017;7:1–11. https://doi.org/10.1038/s41598-017-03591-2.

[31] Lee J, Lee B. Design of thin RC absorbers using a silver nanowire resistive screen. J Electromagn Eng Sci 2016;16:106–11. https://doi.org/10.5515/JKIEES.2016.16.2.106.

[32] Zhang Y, Li T, Chen Q, Zhang H, O'Hara JF, Abele E, et al. Independently tunable dual-band perfect absorber based on graphene at mid-infrared frequencies. Sci Rep 2015;5:1–8. https://doi.org/10.1038/srep18463.

[33] Shen X, Cui TJ, Zhao J, Ma HF, Jiang WX, Li H. Polarization-independent wide-angle triple-band metamaterial absorber. Opt Express 2011;19:9401. https://doi.org/10.1364/oe.19.009401.

[34] Wu C, Neuner B, John J, Milder A, Zollars B, Savoy S, et al. Metamaterial-based integrated plasmonic absorber/emitter for solar thermo-photovoltaic systems. J Opt 2012;14.. https://doi.org/10.1088/2040-8978/14/2/024005.

[35] Simovski C, Maslovski S, Nefedov I, Tretyakov S. Optimization of radiative heat transfer in hyperbolic metamaterials for thermophotovoltaic applications. Opt Express 2013;21:14988. https://doi.org/10.1364/oe.21.014988.

[36] Landy NI, Sajuyigbe S, Mock JJ, Smith DR, Padilla WJ. Perfect metamaterial absorber. Phys Rev Lett 2008;100:1–4. https://doi.org/10.1103/PhysRevLett.100.207402.

[37] Tao H, Landy NI, Bingham CM, Zhang X, Averitt RD, Padilla WJ. A metamaterial absorber for the terahertz regime: design, fabrication and characterization. Opt Express 2008;16:7181. https://doi.org/10.1364/oe.16.007181.

[38] Hedayati MK, Javaherirahim M, Mozooni B, Abdelaziz R, Tavassolizadeh A, Chakravadhanula VSK, et al. Design of a perfect black absorber at visible frequencies using plasmonic metamaterials. Adv Mater 2011;23:5410–4. https://doi.org/10.1002/adma.201102646.

[39] Landy NI, Sajuyigbe S, Mock JJ, Smith DR, Padilla WJ. A Perfect Metamaterial Absorber. Phys Rev Lett 2008;100.. https://doi.org/10.1103/PhysRevLett.100.207402.

[40] M. Luo S. Shen L. Zhou S. Wu Y. Zhou L. Chen Broadband, wide-angle, and polarization- independent metamaterial absorber for the visible regime Opt Express 25 2017 16715 16724 https://doi.org/10.1364/OE.25.016715.

[41] Zhang X, Fan Y, Qi L, Li H. Broadband plasmonic metamaterial absorber with fish-scale structure at visible frequencies. Opt Mater Express 2016;6:2448. https://doi.org/10.1364/ome.6.002448.

[42] Liu J, Liu X, Huang S, Pan P, Chen J, Liu G, et al. Automatically acquired broadband plasmonic-metamaterial black absorber during the metallic film-formation. ACS Appl Mater Interfaces 2015;7:4962–8. https://doi.org/10.1021/acsami.5b00056.

[43] Zhu P, Jay Guo L. High performance broadband absorber in the visible band by engineered dispersion and geometry of a metal-dielectric-metal stack. Appl Phys Lett 2012;101.. https://doi.org/10.1063/1.4771994.

[44] Rufangura P, Sabah C. Dual-band perfect metamaterial absorber for solar cell applications. Vacuum 2015;120:68–74. https://doi.org/10.1016/j.vacuum.2015.05.033.

[45] Abul K. Azad Wilton J.M. Kort-Kamp Milan Sykora Nina R. Weisse-Bernstein Ting S. Luk Antoinette J. Taylor et al. Metasurface broadband solar absorber Opt Mater (Amst) 2016;89:34–41. 10.1016/j.optmat.2018.12.057.

[46] Lai YC, Chen CY, Hung YT, Chen CY. Extending absorption edge through the hybrid resonator-based absorber withwideband and near-perfect absorption in visible region. Materials (Basel) 2020;13.. https://doi.org/10.3390/ma13061470.

[47] Heidari MH, Sedighy SH. Broadband wide-angle polarization-insensitive metasurface solar absorber. J Opt Soc Am A: 2018;35:522. https://doi.org/10.1364/josaa.35.000522.

[48] Li C, Fan H, Dai Q, Wei Z, Lan S, Liu H. Multipole resonance in arrays of diamond dielectric: A metamaterial perfect absorber in the visible regime. Nanomaterials 2019;9.. https://doi.org/10.3390/nano9091222.

[49] Hoa NTQ, Tung PD, Lam PH, Dung ND, Quang NH. Numerical Study of an Ultrabroadband, Wide-Angle, Polarization-Insensitivity Metamaterial Absorber in the Visible Region. J Electron Mater 2018;47:2634–9. https://doi.org/10.1007/s11664-018-6100-5.

[50] Butun S, Aydin K. Structurally tunable resonant absorption bands in ultrathin broadband plasmonic absorbers. Opt Express 2014;22:19457. https://doi.org/10.1364/oe.22.019457.

[51] Abdulkarim YI, Deng L, Muhammad FF, He L. Enhanced light absorption in the organic thin films by coating cross-shaped metamaterial resonators onto the active layers. Results Phys 2019;13:102338 https://doi.org/10.1016/j.rinp.2019.102338.

[52] Mahmud S, Islam SS, Almutairi AF, Islam MT. A Wide Incident Angle, Ultrathin, Polarization-Insensitive Metamaterial Absorber for Optical Wavelength Applications. IEEE Access 2020. https://doi.org/10.1109/ACCESS.2020.3008429.

[53] Shao C, Long H, Cheng Y, Liu X. Low-frequency perfect sound absorption achieved by a modulus- near-zero metamaterial. Sci Rep 2019:1–8. https://doi.org/10.1038/s41598-019-49982-5.

[54] Huang W, Schwan L, Romero-Garcia V, Genevaux JM, Groby JP, 3D-printed straw-inspired metamaterial for sound absorption.. 11th Int Congr Eng Mater Platforms Nov Wave Phenomena. Metamaterials 2017;2017(2017):157–9. https://doi.org/10.1109/MetaMaterials.2017.8107874.

[55] Khuyen BX, Tung BS, Van Dung N, Yoo YJ, Kim YJ, Kim KW, et al. Size-efficient metamaterial absorber at low frequencies: Design, fabrication, and characterization. J Appl Phys 2015;117.. https://doi.org/10.1063/1.4923053.

[56] Hannan Islam, Hoque Singh, Almutairi.. Design of a Novel Double Negative Metamaterial Absorber Atom for Ku and K Band Applications. Electronics 2019;8:853.. https://doi.org/10.3390/electronics8080853.

[57] Yi Z, Lin H, Niu G, Chen X, Zhou Z, Ye X, et al. Graphene-based tunable triple-band plasmonic perfect metamaterial absorber with good angle-polarization-tolerance. Results Phys 2019;13:102149 https://doi.org/10.1016/j.rinp.2019.02.085.

[58] Wang BX, He Y, Xu N, Wang X, Wang Y, Cao J. Design of dual-band polarization controllable metamaterial absorber at terahertz frequency. Results Phys 2020;17:103077 https://doi.org/10.1016/j.rinp.2020.103077.

[59] Baqir MA, Choudhury PK, Member S. Hyperbolic Metamaterial-Based UV Absorber. Technol Lett 2017;1135:1041–135. https://doi.org/10.1109/LPT.2017. 2735453.

[60] Matsuno Y, Sakurai A. Perfect infrared absorber and emitter based on a large-area metasurface. Opt Mater Express 2017;7:618. https://doi.org/10.1364/ome.7. 000618.

[61] Wang BX, Tang C, Niu Q, He Y, Chen T. Design of Narrow Discrete Distances of Dual-/Triple-Band Terahertz Metamaterial Absorbers. Nanoscale Res Lett 2019;14.. https://doi.org/10.1186/s11671-019-2876-3.

[62] Liang C, Zhang Y, Yi Z, Chen X, Zhou Z, Yang H, et al. A broadband and polar-ization-independent metamaterial perfect absorber with monolayer Cr and Ti el-liptical disks array. Results Phys 2019;15:102635https://doi.org/10.1016/j.rinp. 2019.102635.

[63] Qin F, Chen Z, Chen X, Yi Z, Yao W, Duan T, et al. A Tunable Triple-Band Near-Infrared Metamaterial Absorber Based on Au Nano-Cuboids Array. Nanomaterials 2020;10:207. https://doi.org/10.3390/nano10020207.

[64] Shi K, Jin G, Liu R, Ye T, Xue Y. Underwater sound absorption performance of acoustic metamaterials with multilayered locally resonant scatterers. Results Phys 2019;12:132–42. https://doi.org/10.1016/j.rinp.2018.11.060.

[65] Zhao Z, Wang J, Xu C, Yang K, Zhao F, Wang K, et al. Photomultiplication Type Broad Response Organic Photodetectors with One Absorber Layer and One Multiplication Layer. J Phys Chem Lett 2020;11:366–73. https://doi.org/10.1021/ acs.jpclett.9b03323.

[66] Savo S, Shrekenhamer D, Padilla WJ. Liquid crystal metamaterial absorber spatial light modulator for THz applications. Adv Opt Mater 2014;2:275–9. https://doi. org/10.1002/adom.201300384.

[67] Schmidt R, Webb A. Metamaterial Combining Electric-and Magnetic-Dipole-Based Configurations for Unique Dual-Band Signal Enhancement in Ultrahigh-Field Magnetic Resonance Imaging. ACS Appl Mater Interfaces 2017;9:34618–24. https://doi.org/10.1021/acsami.7b06949.

[68] Wang BX, Wang LL, Wang GZ, Huang WQ, Li XF, Zhai X. Theoretical investigation of broadband and wide-angle terahertz metamaterial absorber. IEEE Photonics Technol Lett 2014;26:111–4. https://doi.org/10.1109/LPT.2013.2289299.

[69] Yin S, Zhu J, Xu W, Jiang W, Yuan J, Yin G, et al. High-performance terahertz wave absorbers made of silicon-based metamaterials. Appl Phys Lett 2015;107.. https:// doi.org/10.1063/1.4929151.

[70] G. Duan J. Schalch X. Zhao J. Zhang R.D. Averitt X. Zhang An air-spacer terahertz metamaterial perfect absorber for sensing and detection applications TRANSDUCERS 2017–19th Int Conf Solid-State Sensors, Actuators Microsystems 2017;1:1999–2002. 10.1109/TRANSDUCERS.2017.7994463.

[71] Wang Xiaonong, Luo Chunrong, Hong Gang, Zhao Xiaopeng. Metamaterial optical refractive index sensor detected by the naked eye. Appl Phys Lett 2013;102(9):091902. https://doi.org/10.1063/1.4794170.

[72] Cheng Y, Luo H, Gong R. Triple narrow-band plasmonic perfect absorber for re-fractive index sensing applications of optical frequency. OSA Contin 2019;2(2):2113–22.

[73] Wang BX, He Y, Lou P, Xing W. Design of a dual-band terahertz metamaterial absorber using two identical square patches for sensing application. Nanoscale Adv 2020;2:763–9. https://doi.org/10.1039/c9na00770a.

[74] Wang BX, Wang GZ, Sang T. Simple design of novel triple-band terahertz meta-material absorber for sensing application. J Phys D Appl Phys 2016;49:165307https://doi.org/10.1088/0022-3727/49/16/165307.

[75] Xie J, Zhu W, Rukhlenko ID, Xiao F, He C, Geng J, et al. Water metamaterial for ultra-broadband and wide-angle absorption. Opt Express 2018;26:5052. https:// doi.org/10.1364/oe.26.005052.

[76] Cheng Y, Du C. Broadband plasmonic absorber based on all silicon nanostructure resonators in visible region. Opt Mater (Amst) 2019;98:109441https://doi.org/10. 1016/j.optmat.2019.109441.

[77] A. Shoshi W. Reichl G. Niessner T. Maier H bruckl. Wavelength-Selective Metamaterial Absorber for Thermal Detectors AMA Conf 2015 2015:251–6. 10. 5162/sensor2015/B4..

[78] Zhao H, Ren Y, Fang L, Lin H. Electromagnetic induced transparency in graphene waveguide structure for Terahertz application. Results Phys 2020;16:102971https://doi.org/10.1016/j.rinp.2020.102971.

[79] S.-W. Han J.-W. Kim Y-SS and DPN. Design of infrared wavelength-selective mi-crobolometers using planar multimode detectors Electron Lett 2004;40. 10. 1049/el.

[80] Ghobadi A, Hajian H, Gokbayrak M, Butun B, Ozbay E. Bismuth-based metama-terials: From narrowband reflective color filter to extremely broadband near per-fect absorber. Nanophotonics 2019;8:823–32. https://doi.org/10.1515/nanoph-2018-0217.

[81] Xomalis Angelos, Demirtzioglou Iosif, Jung Yongmin, Plum Eric, Lacava Cosimo, Petropoulos Periklis, Richardson David J, Zheludev Nikolay I. Cryptography in coherent optical information networks using dissipative metamaterial gates. APL Photonics 2019;4(4):046102. https://doi.org/10.1063/1.5092216.

[82] Alam T, Faruque MRI, Islam MT. A double-negative metamaterial-inspired mobile wireless antenna for electromagnetic absorption reduction. Materials (Basel) 2015;8:4817–28. https://doi.org/10.3390/ma8084817.

[83] Lin H, Ye X, Chen X, Zhou Z, Yi Z, Niu G, et al. Plasmonic absorption enhancement in graphene circular and elliptical disk arrays. Mater Res Express 2019;6:45807. https://doi.org/10.1088/2053-1591/aafc3e.

[84] Gong Y, Li Z, Fu J, Chen Y, Wang G, Lu H, et al. Highly flexible all-optical

[85] Niu X, Qi D, Wang X, Cheng Y, Chen F, Li B, et al. Improved broadband spectral selectivity of absorbers/emitters for solar thermophotovoltaics based on 2D pho-tonic crystal heterostructures. J Opt Soc Am A: 2018;35:1832–8.

[86] Wang BX, Wang GZ, Wang LL. Design of a Novel Dual-Band Terahertz Metamaterial Absorber. Plasmonics 2016;11:523–30. https://doi.org/10.1007/ s11468-015-0076-2.

[87] Palik ED. Handbook of Optical Constants of Solids. 1997.

[88] Ghosh G. Dispersion-equation coefficients for the refractive index and bi-refringence of calcite and quartz crystals. Opt Commun 1999;163:95–102. https:// doi.org/10.1016/S0030-4018(99)00091-7.

[89] Philip M, Schneider Fowler WB. Band Structure and Optical Properties of Silicon Dioxide. Phys Rev Lett 1976;36:8–11.

[90] Zhang C, Zhou W, Sun S, Yi N, Song Q, Xiao S. Absorption enhancement in thin-film organic solar cells through electric and magnetic resonances in optical me-tamaterial. Asia Commun Photonics Conf ACPC 2015;2015(5):1954–61. https:// doi.org/10.1364/ome.5.001954.

[91] Cheng Y, Chen F. Triple-Band Perfect Light Absorber Based on Hybrid Metasurface for Sensing Application. Nanoscale Res Lett 2020.

[92] Cui Yanxia, Fung Kin Hung, Xu Jun, Ma Hyungjin, Jin Yi, He Sailing, Fang Nicholas X. Ultrabroadband Light Absorption by a Sawtooth Anisotropic Metamaterial Slab. Nano Lett 2012;12(3):1443–7. https://doi.org/10.1021/ nl204118h.

[93] H.L. Huang H. Xia Z.B. Guo D. Xie H.J. Li Design of Broadband Metamaterial Absorbers for Permittivity Sensitivity and Solar Cell Application Chinese Phys Lett 2017;34. 10.1088/0256-307X/34/11/117801.

[94] Cai W, Chettiar UK, Kildishev AV, Shalaev VM. Optical cloaking with metama-terials. Nat Photonics 2007;1:224–7. https://doi.org/10.1038/nphoton.2007.28.

[95] Y.Z. Cheng Z.Z. Cheng X.S. Mao R.Z. Gong Ultra-thin multi-band polarization-in-sensitive microwave metamaterial absorber based on multiple-order responses using a single resonator structure Materials (Basel) 2017;10. 10.3390/ ma10111241.

[96] C. Cao Y. Cheng Quad-Band plasmonic perfect absorber for visible light with a patchwork of silicon nanorod resonators Materials (Basel) 2018;11. 10.3390/ ma11101954.

[97] Cao C, Cheng Y. A broadband plasmonic light absorber based on a tungsten meander- ring-resonator in visible region. Appl Phys A 2019. https://doi.org/10. 1007/s00339-018-2310-1.

[98] Wang B, Wang G, Sang T, Wang L. Six-band terahertz metamaterial absorber based on the combination of multiple-order responses of metallic patches in a dual-layer stacked resonance structure. Nat Publ Gr 2017:1–9. https://doi.org/10.1038/ srep41373.

[99] B.X. Wang Quad-band terahertz metamaterial absorber based on the combining of the dipole and quadrupole resonances of two SRRs IEEE J Sel Top Quantum Electron 2017;23. 10.1109/JSTQE.2016.2547325.

[100] Wang BX, Wang GZ, Wang LL, Zhai X. Design of a five-band terahertz absorber based on three nested split-ring resonators. IEEE Photonics Technol Lett 2016;28:307–10. https://doi.org/10.1109/LPT.2015.2495245.

[101] Y. Qi Y. Zhang C. Liu T. Zhang B. Zhang L. Wang et al. A tunable terahertz me-tamaterial absorber composed of hourglass-shaped graphene arrays Nanomaterials 2020;10. 10.3390/nano10030533.

[102] Y.I. Abdulkarim L. Deng H. Luo S. Huang L. He L. Yuhan et al. Electromagnetic simulations of polarization-insensitive and wide-angle multiband metamaterial absorber by incorporating double asterisk resonator Bull Mater Sci 2020;43. 10. 1007/s12034-020-02098-3.

[103] Li W, Guler U, Kinsey N, Naik GV, Boltasseva A, Guan J, et al. Refractory plas-monics with titanium nitride: Broadband Metamaterial Absorber. Adv Mater 2014;26:7959–65. https://doi.org/10.1002/adma.201401874.

[104] Rothwell EJ, Frasch JL, Ellison SM, Chahal P, Ouedraogo RO. Analysis of the Nicolson-Ross-Weir method for characterizing the electromagnetic properties of engineered materials. Prog Electromagn Res 2016;157:31–47. https://doi.org/10. 2528/PIER16071706.

[105] Gasimov N, Karaaslan M, Sabah C, Karadag F. Some aspects of mass-energy equivalence which appears in left-handed metamaterials. EPJ Appl Metamaterials 2019;6:1–5. https://doi.org/10.1051/epjam/2019013.

[106] H.M. Lee J.C. Wu A wide-angle dual-band infrared perfect absorber based on metaldielectricmetal split square-ring and square array J Phys D Appl Phys 2012;45. 10.1088/0022-3727/45/20/205101.

[107] Cao T, Zhang L, Simpson RE, Cryan MJ. Mid-infrared tunable polarization-in-dependent perfect absorber using a phase-change metamaterial. J Opt Soc Am B 2013;30:1580. https://doi.org/10.1364/josab.30.001580.

[108] Han X, He K, He Z, Zhang Z. Tungsten-based highly selective solar absorber using simple nanodisk array. Opt Express 2017;25:A1072. https://doi.org/10.1364/oe. 25.0a1072.

[109] Liu N, Mesch M, Weiss T, Hentschel M, Giessen H. Infrared perfect absorber and its application as plasmonic sensor. Nano Lett 2010;10:2342–8. https://doi.org/10. 1021/nl9041033.

[110] Zhang H, Guan C, Luo J, Yuan Y, Song N, Zhang Y, et al. Facile Film-Nanoctahedron Assembly Route to Plasmonic Metamaterial Absorbers at Visible Frequencies. ACS Appl Mater Interfaces 2019;11:20241–8. https://doi.org/10. 1021/acsami.9b01088.